
140
460
THS

This is to certify that the
thesis entitled

MICROCHIP SEPARATIONS OF ALKALOIDS
WITH UV-ABSORBANCE SPECTRAL DETECTION

presented by

Carl Isaac Downey Newman

has been accepted towards fulfillment
of the requirements for the

M.S. degree in Criminal Justice

Major Professor's Signature

2nd July 2007.

Date

DATE DUE	DATE DUE	DATE DUE

MICROCHIP SEPARATIONS OF ALKALOIDS WITH UV-ABSORBANCE SPECTRAL DETECTION

By

CARL ISAAC DOWNEY NEWMAN

A THESIS

Submitted to
Michigan State University
in partial fulfillments of the requirements
for the degree of

MASTER OF SCIENCE

Criminal Justice

2007

ABSTRACT

MICROCHIP SEPARATIONS OF ALKALOIDS
WITH UV-ABSORBANCE SPECTRAL DETECTION

By

Carl Isaac Downey Newman

In this work, a microchip device is developed for the electrophoretic separation and UV-absorbance spectral detection of four toxic alkaloids: colchicine, aconitine, strychnine, and nicotine. This is achieved by fabricating and employing fused-silica (quartz) microchips with a simple, cross geometry for separations and a miniature, fiber-optic CCD spectrometer for detection. UV-absorbance detection is achieved with these microchips as a result of the optical properties of the quartz substrate and facilitated by employing an etched bubble-cell to increase pathlength as well as by application of micelle stacking to affect on-line sample enrichment. A miniature CCD spectrometer configured for detecting UV light is used to monitor separations over a user specified spectral range. Thus, qualitative and quantitative separations are achieved by resolving solutes spatially as well as spectrally. Figures of merit to include reproducibility and limits of detection are discussed and a simulated, forensic application to spiked, real-world beverages is demonstrated.

To my family . . .

. . . and in loving memory of Marshall -
the sweetest and happiest four-toothed dog
that I have ever known.

ACKNOWLEDGEMENTS

Much gratitude is owed to those who have aided and inspired me towards this accomplishment. To Dr. Walter Birkby at the University of Arizona and Dr. Glen Doran at the Florida State University who fostered and facilitated my nascent undergraduate interest in forensic science as well as the general application of science to help others. To Professor Victoria McGuffin at the Michigan State University for all her efforts to make me a better scientist and teaching me to never lose sight of "the big picture". To Drs. Greg Collins, Qin Lu, and Braden Giordano at the U.S. Naval Research Laboratory in Washington, DC for their thoughtful discussion and for being generally fun people to do science with. To Professor Ruth Waddell at the Michigan State University for her candor and guidance . . . and for keeping the faith in my eventual, albeit circuitous, completion of this degree. Finally, to my wife, Haruko, for her unconditional love and support and for her patience with me as I pursued my graduate education.

TABLE OF CONTENTS

LIST OF TABLES

LIST OF FIGURES

CHAPTER 1

INTRODUCTION AND BACKGROUND

1.1 *Alkaloids.*

Alkaloids are naturally occurring plant products that have numerous applications in veterinary and human medicine at low doses and are typically toxic in large doses. For example, colchicine is produced naturally in meadow saffron (*Colchicum autumnale L.*) and used in human and veterinary medicine for treatment of papillomas and warts in cattle and horses, as well as in human medicine for treatment of gout arthritis [1]. However, overdose can lead to vomiting, nausea, diarrhea, attenuated lactation, and death [2,3]. Similarly, aconite plants (*Aconitum sp.*) produce numerous different alkaloids. The roots and the processed products of aconite roots have been used in Chinese herbal medicines for their anti-inflammatory, analgesic, and cardiotronic properties. However, large doses can result in death from ventricular arrhythmia or cardiac paralysis [4].

Traditionally, alkaloids have been defined as naturally occurring amines produced via plant biosynthesis but the term has been extended to include those amines produced by animals and fungi as well [5]. These molecules are usually classified according to their respective metabolic pathways of construction; however, they were historically grouped with similarly structured molecules (e.g. opium alkaloids group with phenanthrenes) or by the organism from which they were first isolated (e.g. nicotine from *Nicotiana tabacum*). [6] Many alkaloids are

poisonous and all are basic in character, each containing a heterocyclic nitrogen. Otherwise, these molecules exhibit broad chemical and physical diversity [7]. As a result of their toxic properties, development of a sensitive, selective, and potentially portable method of screening for alkaloids in foods, beverages, and dietary supplements is critical to mitigating accidental inclusion, as well as attempted bioterrorism.

There are currently several primary methods employed for the separation and detection of alkaloids. Most of these methods utilize liquid or gas chromatography for separation, coupled with either UV absorbance or mass spectrometry for detection [7-11]. There have also been several reports of capillary electrophoresis (CE) separations of alkaloids with UV absorbance detection [12-15].

1.2 *Overview of Capillary Electrophoresis Separations*

1.2.1 Capillary Electrophoresis

Electrophoresis is the separation of charged molecules or particles by differential migration in an electric field. The first reported use of electrophoresis as a separation technique was in the 1930s by Tiselius for the separation of constituent proteins from human serum [16, 17]. This pioneering work eventually earned Tiselius the Nobel Prize in 1948.

Electrophoresis in a glass capillary was first reported by Hjerten in 1967 [18], but did not gain popularity until some 14 years later when Jorgenson and Lukacs [19] demonstrated the efficiency of the technique for separating small

biological molecules. In the intervening years, capillary electrophoresis (CE) and related techniques has become a staple for fast and efficient separations of charged and neutral solutes. Applications of CE include trace analysis of metals from environmental samples and protein separations for the Human Genome Project [20]. A recent review by Issaq [21] discusses a broad range of solutes for which separation by CE has become standard operating procedure.

Typically in CE, small volumes (1-10 nL) of analyte are injected either hydrodynamically or electrokinetically into a capillary and separation is achieved as a result of differential and concurrent migration within the bulk solution (background electrolyte) under the influence of an applied electric field. Physical origins of this unique separation mechanism are derived from the formation of an electrical double-layer at the interface of the bulk solution and the capillary walls, combined with the mass transfer response of solute and bulk components in an electric field. Chemical origins of the separation originate from acid-base equilibria, complexation equilibria, and wall adsorption.

These physical and chemical contributions to CE separation are manifest in the observed velocity (v_{obs}) of individual analytes by

$$v_{obs} = v_{ep} + v_{eo} \qquad (1)$$

where v_{ep} is the electrophoretic velocity of the analyte and v_{eo} is the electroosmotic velocity of the bulk solution. Electrophoretic velocity is solute-specific and is dictated primarily by the ratio of analyte charge (z) to size (r) as well as any chemical interactions it experiences during the separation.

Conversely, electroosmotic velocity is system specific and is dictated by the properties of the bulk solution and the capillary surface.

Figure 1.1 illustrates the separation mechanism and relative elution order of charged and neutral analytes in CE. Typically bulk flow travels away from the applied positive high voltage and towards electrical ground at the electroosmotic velocity. Neutral molecules have no net charge (z/r = 0) and therefore travel with bulk flow. Positively charge molecules, on the other hand, travel more rapidly than the bulk (z/r > 0); with analytes exhibiting larger charge-to-size ratios eluting more rapidly than analytes with smaller charge-to-size ratios. Conversely, negatively charged molecules, travel slower than the bulk (z/r < 0); with analytes exhibiting smaller charge-to-size ratios eluting more rapidly than analytes with larger charge-to-size ratios.

Many analytes in CE are subject to acid-base equilibria. Consequently, the v_{ep} of these solutes is pH dependent and may be described as a function of the analyte acid dissociation constant (K_a) values and the pH of the bulk solution

$$v_{ep} = \sum v_{i,z}\alpha_{i,z} \qquad (2)$$

Where $\alpha_{i,z}$ is the fraction of analyte i molecules existing with charge state z. For analyte molecules undergoing a simple, one-proton equilibrium such as

$$A^- + H^+ \leftrightarrow AH \qquad (3)$$

the electrophoretic velocity can be expressed as

$$v_{ep} = \frac{v_{A-} + K_a[H^+]v_{AH}}{1 + K_a[H^+]} \qquad (4)$$

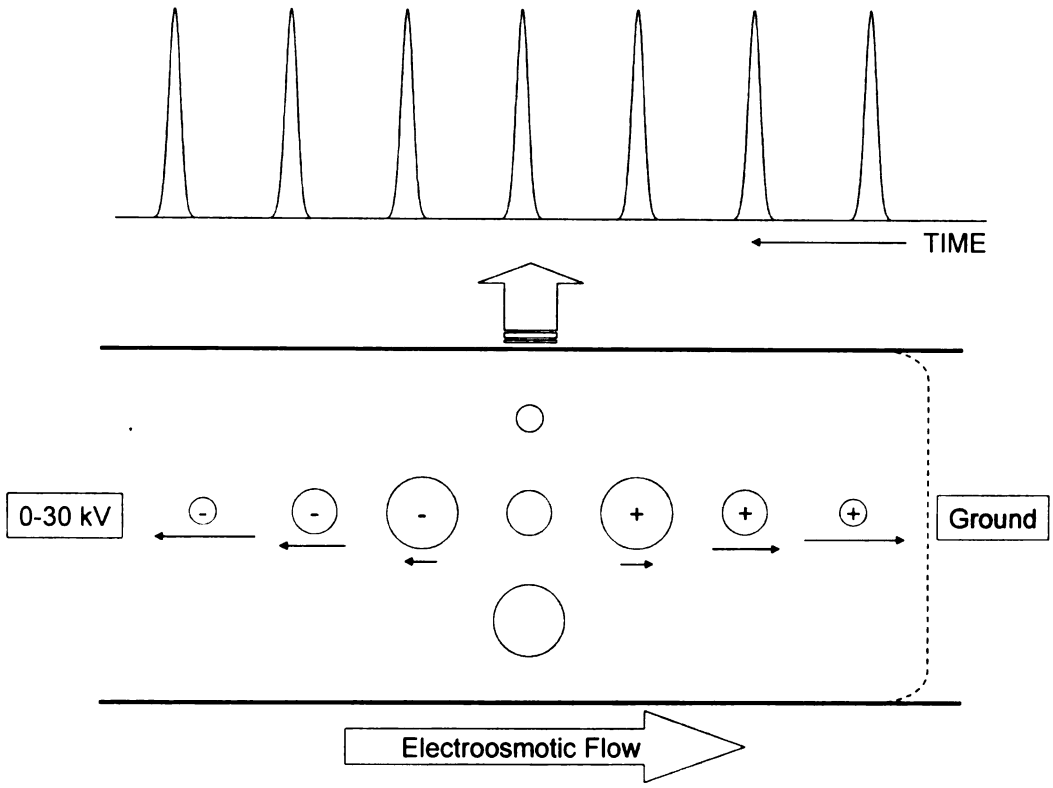

Figure 1.1: Illustration of separation mechanism and relative elution order of charged and neutral analytes in CE. Bottom: solid, parallel lines represent capillary walls; dashed, curved line represents bulk flow profile; arrows beneath analyte molecules represent relative vectors of v_{ep}. Top: representative electropherogram of separation of analytes depicted. Analyte molecules separate based on intrinsic charge-to-size ratio and bulk (electroosmotic flow) in an applied electric field. Positive analytes elute first in order of increasing z/r, followed by neutral analytes, and then negative analytes in order of decreasing z/r.

where v_{A^-} and v_{AH} are the electrophoretic velocities of the unprotonated and protonated analyte, respectively.

1.2.2 Micellar Electrokinetic Chromatography

Micellar electrokinetic chromatography (MEKC) is used to achieve separation of neutral (and otherwise unresolveable) analytes in CE. This is achieved by providing neutral analytes the opportunity to partition into the core of a charged micelle, thereby effecting a change in the v_{obs} of the analyte.

Figure 1.2 illustrates the equilibrium for a neutral analyte molecule undergoing reversible partitioning between the bulk and a negatively-charged micelle traveling more slowly than v_{eo}. Consequently, as the equilibrium constant (K) for analyte partioning into the micelle increases, v_{obs} decreases, and analyte elution time increases.

Mathematically, this trend is identical to that for the pH dependence of v_{obs} discussed in the previous section (Equation 4). However, for MEKC the description of v_{ep} is greatly simplified because neutral analytes exhibit no net charge – and hence no native electrophoretic mobility. Thus, the observed velocity for neutral analytes in MECK is effectively reduced to

$$v_{obs} = v_{eo} + \frac{K[MC]v_{mc}}{1+K[MC]} \qquad (5)$$

where [MC] is the micelle concentration and v_{mc} is the velocity of the analyte in the micelle (typically equivalent to the velocity of the micelle). Thus, analytes with small K values exhibit velocities dominated by v_{eo}; whereas, analytes with large K values exhibit velocities dominated by v_{mc}.

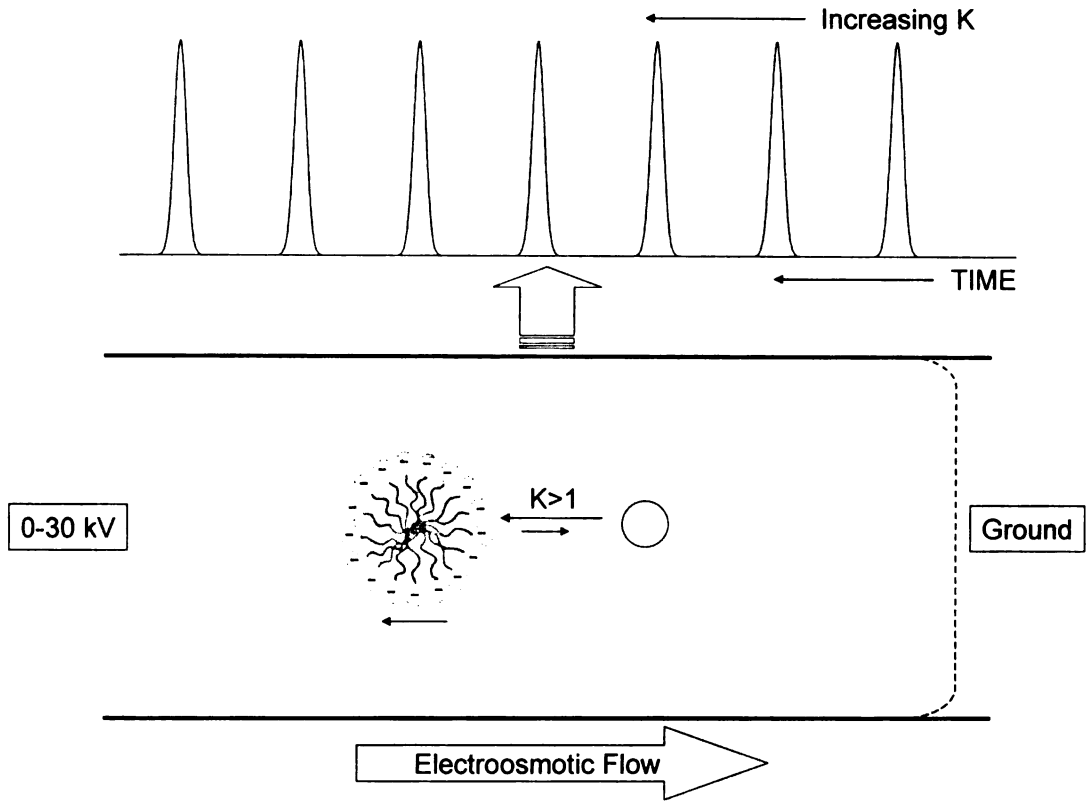

Figure 1.2: Illustration of separation mechanism and relative elution order neutral analytes in MEKC. Bottom: solid, parallel lines represent capillary walls; dashed, curved line represents bulk flow profile; arrow beneath micelle represents relative vector of v_{mc}; forward and reverse reaction arrows represent reversible equilibrium of analyte partitioning between bulk and micelle. Top: representative electropherogram of MEKC separation of neutral analytes with increasing K. Analyte molecules separate based on intrinsic partition coefficient for micelle and bulk (electroosmotic flow) in an applied electric field. Analytes with smaller K values elute earlier and analytes with larger K values elute later.

1.3 *Microchip Detection Methods.*

Whereas the capillaries used in CE separations afford the application of numerous detection platforms (i.e. absorbance, fluorescence, electrochemical, mass spectrometry, etc.) their scale effectively precludes operation beyond the bench-top. However, the compact dimensions of the microchip separation platform make portability practical. Microchip-based capillary electrophoresis devices have predominantly been limited to either electrochemical or fluorescence detection methods. However, most alkaloids lack sufficient aromatic structure for fluorescence detection and the caustic conditions required for voltammetric detection (e.g. pH 2.7 for colchicine) are not well suited to microchip separations [22,23]. On the other hand, whereas many alkaloids absorb UV light, this method of detection has been of negligible utility on the microchip platform because of the prohibitively small path lengths inherent with such devices and the resulting poor sensitivity. Cramer et al. demonstrated, for example, that the trapezoidal-shaped channels etched in glass substrates result in an effective pathlength that is approximately 50% that of the etched depth [24]. For a typical channel depth of 20 μm, reducing this to an effective pathlength of ~10 μm becomes a serious sensitivity issue for absorbance detection.

Consequently, several methods for increasing the path length on a CE microchip have been examined. Harrison and co-workers achieved absorbance detection of 6 μM fluorescein isothiocyanate by fabricating a U-cell (120-140 μm long) within the plane of the glass microchip device [25]. Absorbance of 633 nm light by 50mM bromothymol blue was achieved via fabrication of a multi-reflection

cell within the microchip that resulted in effective optical pathlengths of 50-272 μm [26]. Morgensen et al. achieved absorbance of 488 nm light by 3.2 μM Rhodamine 110 by fabricating optical waveguides into a silicon, planar microchip with a 750 μm U-cell [27]. Collins et al. demonstrated absorbance of 660 nm light by metallochromic, transition metal chelates in 20 μm and 100 μm uniformly deep channels [28,29]; and later, of 525 nm light by 20.3 μM Rhodamine B by fabricating a 3-dimensional, separation channel with a 126 μm pathlength [30]. Lu et al. showed absorbance of 350 nm light by 50 μM colchicine with discrete lengths of increased channel depth (65 & 115 μm) (re: etched "bubble cells") [31]. Finally, Giordano et al. demonstrated absorbance of 254 nm light by nitrated explosives on a fused-silica microchip with a 100 μm etched "bubble cell" and on-line pre-concentration via an alkyl modified sol-gel [32]. Whereas uniformly large channels necessitate non-aqueous buffer compositions to mitigate Joule heating effects, application of a "bubble cell" confines the increased channel dimensions to a discrete region, effectively attenuating additional contributions to Joule heating due to increased feature size.

1.4 *On-line Sample Enrichment.*

In addition to increasing the optical pathlength to achieve increased detection sensitivity, chemically facilitated sensitivity enhancements via on-line sample enrichment in CE and microchip-CE have been a topic of much discussion [33-45]. Moreover, on-line sample enrichment in CE separations has been the subject of numerous reviews in the recent literature [46-51]. For neutral

analytes, such as alkaloids, these separations are achieved via micellar electrokinetic chromatography (MEKC). Hence, with this mechanism, on-line sample enrichment can be achieved by the concerted effects of a velocity gradient [34] as well as on-line micelle pre-concentration ("micelle stacking") [37].

Several groups have presented on-column sample pre-concentration methods for MEKC including high salt stacking, field amplified stacking, and sweeping [33,34,37]. Recently, Giordano and co-workers have expanded the discussion of micelle stacking in MEKC and its effect on separations of neutral analytes [45]. It was concluded that micelle stacking is an intrinsic contribution to each of the pre-concentration methods mentioned above, and that extensive micelle stacking can result in both enhanced sensitivity and resolution in MEKC.

These advantages are illustrated well in Figure 1.3 by the separation of a mixture of 5 alkaloids via stacked cholate micelles. Each electropherogram represents separations achieved after 45 cm of separation distance for injection length of 5 – 45 mm (bottom to top). Each trace also lists the full peak width (FW) for a moderately retained analyte as well as the resolution (R_s) of the limiting pair. It is clear that signal intensity increases with injection length without any substantive increase in peak width. The net effect of these trends is that, counter to chromatographic wisdom and the wont of entropic forces, increased injection length and hence, increased sample mass, can, in fact, afford increased resolution. This is possible because of the generation of a narrow zone of

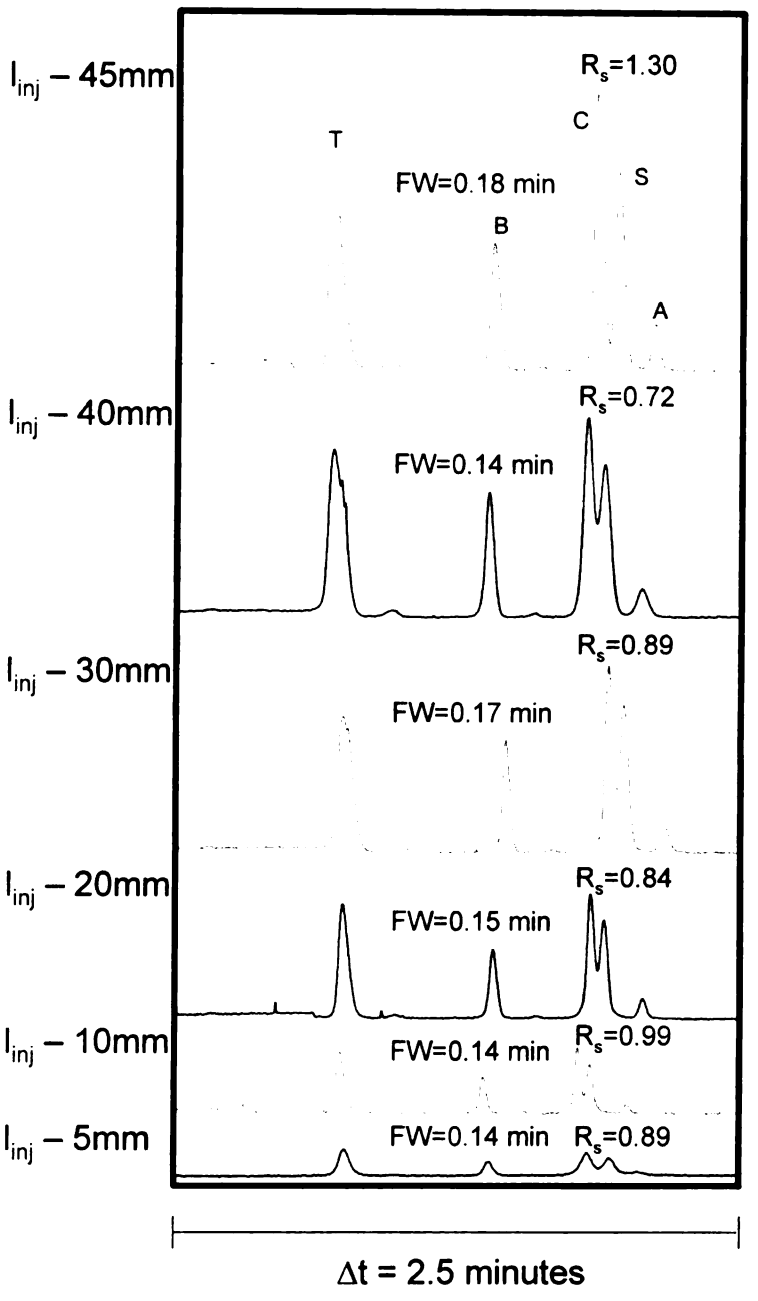

Figure 1.3: Effect of injection length (l_{inj}) on the separation, peak width, and resolution of 5 alkaloids: 13 μM thiocolochicoside (T) and benzion methyl ether (B), 17 μM colchicine (C) and strychnine (S), and 43 μM aconitine (A) from [45]. Experimental conditions: L_T = 60 cm (45 cm effective length), l_{inj} = 5 – 45 mm, V = 25 kV. BGE = 10 mM sodium tetraborate, 80 mM sodium dodecyl sulfate, sample matrix = 10 mM sodium tetraborate.

artificially high micelle concentration (stacked micelles) that facilitates the on-line enrichment of analyte molecules. A cartoon of the micelle stacking phenomenon and its effect on sample enrichment is shown in Figures 1.4A-D.

1.5 *Research Objectives*

The objective of this research is to develop a CE microchip device capable of UV-absorbance spectral detection and to optimize experimental conditions to facilitate separation and detection of toxic alkaloid mixtures of aconitine, colchicine, nicotine, and strychnine.

Consequently, this work requires not only instrumental design of the CE microchip device in order to perform the requisite measurements, but also experimental design in order to determine optimal separation conditions as well as extraction procedures for analyzing alkaloids spiked into various beverage matrices.

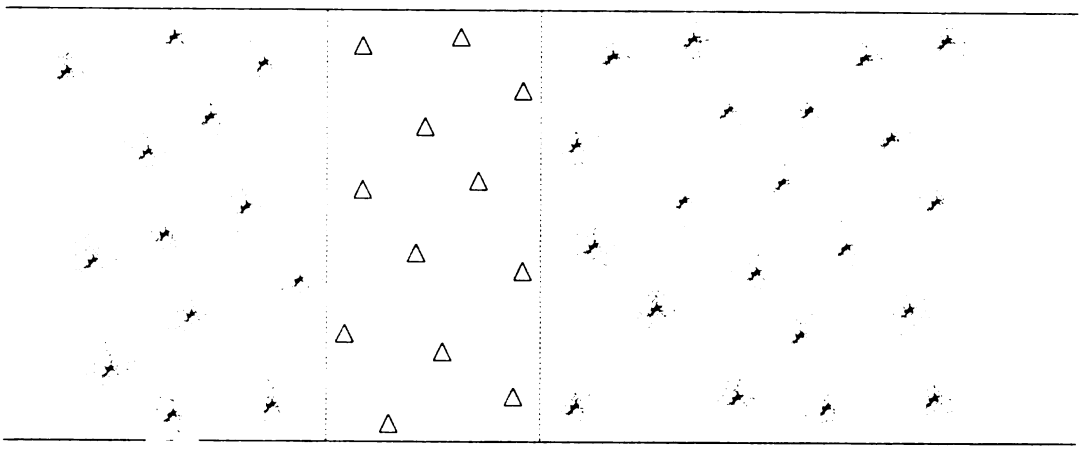

Figure 1.4A: Analyte (triangles) in sample matrix is injected as discrete plug (dashed vertical lines) into micelle-containing background electrolyte.

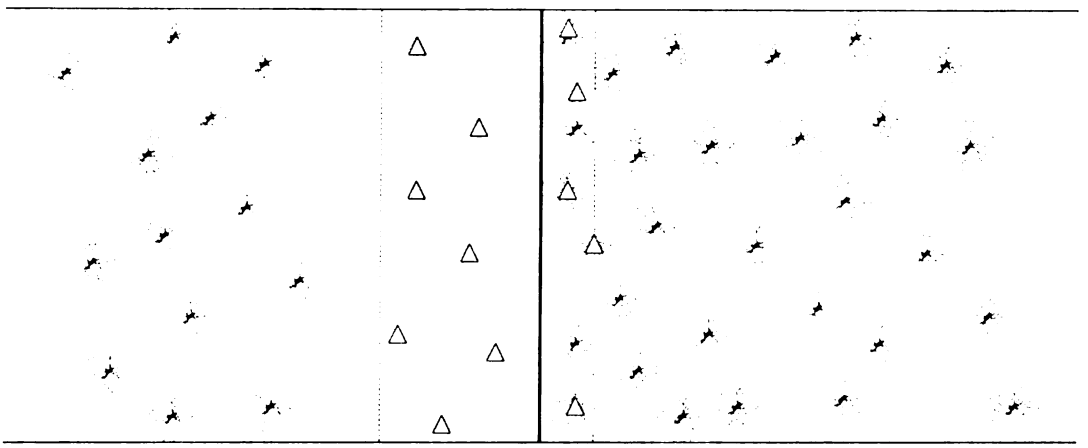

Figure 1.4B: Micelles stacking initiates against boundary formed at interface of background electrolyte and sample matrix. Analyte enters micelle region and concentrates as a result of artificially high equilibrium constant (stacked micelles) and velocity gradient between electroosmotic flow and micelle velocity.

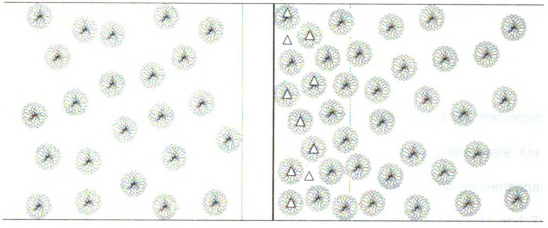

Figure 1.4C: Micelles continue to stack, increasing an already artificially high local micelle concentration. Analyte continues to concentrate in stacked micelle region and begins to separate from sample matrix.

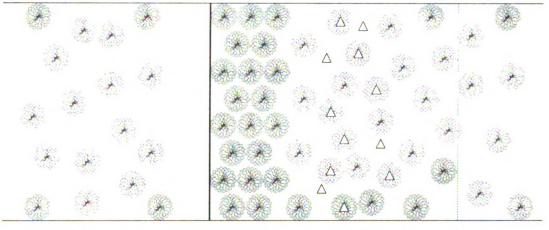

Figure 1.4D: Micelles continue to stack, increasing an already artificially high local micelle concentration. Concentrated analyte exits stacked micelle region and establishes equilibrium with basal micelle concentration. Analyte is completely separated from sample matrix.

CHAPTER 2

INSTRUMENT DEVELOPMENT

2.1 *Introduction*

This chapter describes the instrumental development of a CE microchip device for UV-absorbance spectral detection. Until recently there were two fundamental, physical impediments to UV-absorbance detection on conventional microchip devices: 1) poor UV transmittance of conventional substrates and 2) extremely short detection pathlength. These problems are addressed individually in this chapter. First, whereas microchip CE devices are typically constructed from glass or hard plastic, it is necessary to utilize a fused-silica substrate in order to achieve UV absorbance detection. Second, an etched "bubble cell" is fabricated in order to address the geometry-attenuated pathlength inherent to microchip devices.

Additionally, a series of optical elements are used to transmit and focus light from a UV light source, through the microchip, and finally to a portable CCD spectrometer. The effect of this controlled optical path is to maximize the total amount of UV light transmitted to and collected through the microchip, while minimizing the total amount of background light that is measured. Thus, the net result of this combined approach to instrumental design is dichotomous. Microchip fabrication is used to maximize signal by increasing the optical pathlength and UV throughput; whereas the detection scheme is used to minimize noise by attenuating contributions from background or ambient light.

The miniature CCD is used to collect transmitted light and record the UV-absorbance spectra at each point in the separation. This detection method affords increased sensitivity by affording simultaneous detection at multiple wavelengths as well as spectral resolution that provides a measure of orthogonality to the spatial resolution of the separation and facilitates solute identification by UV-absorbance spectra.

2.2 *Quartz Microchip Design and Fabrication.*

2.2.1 Microchip Design.

Design of the microchip device consisted of a simple, cross-T geometry for injection and separation, coupled with a "bubble cell" for detection. In order to achieve this design, complimentary patterns were etched into the top and bottom substrates of the device. The top substrate contained a simple, cross-T pattern and the bottom substrate contained a short channel that, when aligned properly, resulted in a small "bubble" in the separation channel centered about 4.5 cm from the injection point. The cross-T geometry in the top substrate consists of three shorter arms each 2 cm in length that intersect a fourth, longer arm that is 8 cm in length. The intersection point of these arms facilitates the establishment of a fluidic gate between sample and buffer flow regimes that can be used to achieve reproducible injections. The "bubble" geometry in the bottom substrate consists of a short (1 mm) channel that, when overlaid by the separation channel, serves to increase the optical pathlength for absorbance detection.

2.2.2 Quartz Microchip Fabrication.

Microchips were fabricated from 4" x 4" x 0.09" quartz wafers pre-coated on one side with chrome and AZ1500 photoresist (Nanofilm, Westlake Village, CA). Dimensions of the completed microchip are shown in Figure 2.1. Standard photolithography and wet chemical etching were used to fabricate the device, and the final channel depths for both substrates were ~25 μm deep.

Briefly, coated quartz wafers were cleaned with Ar(g), covered with a patterned photomask, and exposed to a 200 W Xe lamp for 90 seconds. The exposed photoresist and underlying chrome were removed sequentially by 0.1 M NaOH, water, and then Chromium Etchant Type 1020 (Transense Company Inc., Danvers, MA). The patterned wafers were then baked at 100 °C for ~ 15 minutes and allowed to cool to room temperature. Cooled wafers were etched in Buffered Oxide Etchant 6:1 (Transverse Company Inc., Danvers, MA) for ~3.5 hour at 25 °C. The etched wafers were rinsed with water before fabricating reservoir access holes with 1.4 mm triple ripple diamond drill bits (Crystalite Corporation, Lewis Center, OH) with a mounted variable-speed dremel (2.0 amp, Craftsman, Sears Brands, USA.).

The remaining photoresist and chrome layers were removed and the etched pieces were placed in a bath of 30% Branson cleaning solution (Branson, Danbury, CT) and sonicated for 30 minutes. The pieces were then sonicated for 30 minutes in filtered water (Millipore, Billerica, MA). The surface of each substrate was then prepared for bonding using a procedure modified

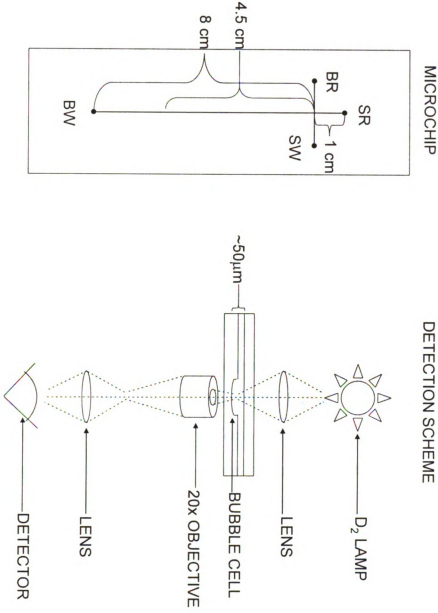

Figure 2.1: Dimensions of quartz microchip and schematic illustration of detection system set-up. SR = sample reservoir; SW = sample waste; BR = buffer reservoir; BW = buffer waste.

from LIGO Drawing # E050228-00-D [52] and previously described in detail by Giordano et al. [32].

For bonding, 5 mL of a 4:1 *v/v* solution of water to sodium silicate solution (Sigma-Aldrich, St. Louis, MO) was centrifuged for 4 minutes at 10,000 rpm (Eppendorf, Westbury, NY). The supernatant of the resulting solution was placed into a 3 mL syringe, and approximately 1 mL of the bonding solution was filtered through a 0.2 μm filter (Fisher Scientific, Pittsburg, PA) directly onto the bottom plate. The top plate was brought into contact such that no air bubbles were visible when pressed together. After alignment of the two plates to orient the "bubble" in the channel structure, the plates were allowed to rest for ten minutes, creating a temporary bond. After bonding, a vacuum was used to remove the bonding solution filling the channel structure. The channel was then rinsed with 0.1 M NaOH and then water, by vacuum. Once all of the liquid was removed from the channels, the device was baked at 100 °C under light pressure for 48 hours to create a permanent bond. Final dimensions of the "bubble cell" were typically 1 mm long x 95 μm wide x 50 μm deep.

2.3 *Microchip UV-Absorbance Detection System Design and Instrumentation.*

2.3.1 Optical Design

A series of UV-grade optical fibers and focusing optics were used to maximize the transmission and collection of light through the microchip device for UV absorbance detection. Radiant output from a 30 W deuterium lamp was

carried via solarized, UV-grade optical fiber (400 μm core, Ocean Optics, Denedin, FL) to a focusing beam probe containing a series of plano-convex, fused-silica lenses (Newport Stratford Inc., Stratford, CT) which first collimates light from the optical fiber and then focuses that light into the "bubble cell" of the microchip. Transmitted light was collected with a quartz microscope objective (20 x 0.65, Partec GmbH, Munster, Germany) and transmitted through a 1000 μm pinhole into a second series of plano-convex, fused-silica lenses that focus the light into a second solarized, UV-grade optical fiber which then carries the light to the detector. A schematic illustration of the detection scheme is shown in Figure 2.1.

2.3.2 Detector Instrumentation and Software

UV absorbance was detected via a miniature CCD spectrometer (HR2000 High-Resolution Mini-Spectrometer, Ocean Optics). The CCD spectrometer utilizes a 2048-pixel array and is firmware-configured to detect light between 190 – 645 nm. The spectrometer is interfaced to commercially available software (LabView, National Instruments, Austin, TX) via proprietary drivers (Ocean Optics) that enable visualization of collected spectra in real-time. This software was then modified to display collected data between 210 – 400 nm in real-time as spectra and as individual time-dependent signals at ~4.5 nm intervals. The modified data collection program records absorbance spectra (210 – 400 nm) at ~15 Hz, assigns a time-stamp to each recorded spectrum, and the data are written to file as tab-delimited ASCII text along with any relevant experimental

details provided by the user. A screen-shot of the front-panel for the data collection program is shown in Figure 2.2.

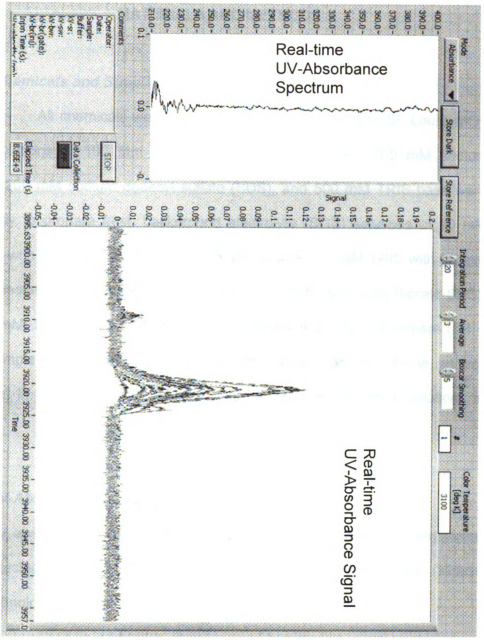

Figure 2.2: Screen-shot of front panel for data collection program.

CHAPTER 3

MATERIALS AND METHODS

3.1 *Chemicals and Supplies.*

All chemicals were purchased from Sigma-Aldrich (St. Louis, MO). Stock solutions of 100 Mm sodium tetraborate ($Na_2B_4O_7$), 200 mM sodium cholate, 200 mM sodium dodecyl sulfate (SDS), and 500 mM TRIS base were used daily to prepare fresh background electrolyte (BGE) solutions of 10 mM $Na_2B_4O_7$ with 80 mM sodium cholate (borate-cholate), 10 mM TRIS with 80 mM sodium cholate (TRIS-cholate), 10 mM $Na_2B_4O_7$ with 80 mM SDS (borate-SDS), and 10 mM TRIS with 80 mM SDS (TRIS-SDS) without pH adjustment (pH ~ 9.5). Sample solutions of aconitine, colchicine, nicotine, and strychnine, as well as Sudan III and Rhodamine B were prepared from 5 mM stock solutions in alcohol.

3.2 *UV-Absorbance Spectra.*

UV absorbance spectra of aconitine, colchicine, nicotine, and strychnine were collected with a double-beam spectrophotometer (Model U-3000, Hitachi High Technologies, San Jose, CA).

3.3 *Solid-Phase Extraction Procedures.*

SPEC-PLUS-3ML-DAU solid-phase extraction (SPE) columns (Varian, Inc., Lake Forest, CA) were used to recover alkaloids from spiked samples via a

modification of the manufacturers recommended procedure for the extraction of codeine and morphine from urine. Specifically, 10 mL of water, juice, or milk was spiked with 30 μM each of nicotine, aconitine, colchicine, and strychnine and acidified by adding 2 mL of 1 M HNO_3. The milk sample was briefly centrifuged to isolate coagulated solids prior to SPE of the liquid portion. The SPE column was washed with 200 μL of methanol prior to loading the spiked sample. The column was then rinsed with 1 mL of 1 M HNO_3 and dried under vacuum for 5 minutes. One mL of freshly made elution solvent containing 2% NH_4OH, 20% methanol, and 78% ethyl acetate was used to elute the alkaloids from the SPE column. The eluent was evaporated to dryness and reconstituted in 0.6 mL of sample matrix prior to analysis.

3.4 *Experimental Systems.*

Two experimental systems were employed to perform the work described in this thesis. A commercially available CE instrument with auto-sampling capabilities was utilized to facilitate identification of appropriate background electrolyte and sample matrix combinations for separations. These separation conditions were then investigated to determine their efficacy after translation to the microchip device designed and constructed in-house.

3.4.1 Capillary Electrophoresis Instrumentation

Capillary separations were performed with a Beckman Coulter P/ACE MDQ capillary electrophoresis instrument equipped with an auto-sampler and a

UV absorbance detector (Fullerton, CA). Samples were injected hydrodynamically (0.5 psi) into a 50 μm i.d. x 360 μm o.d. fused-silica capillary (PolyMicro, Phoenix, AZ) and separations were then achieved with applied potentials of 15 - 25 kV. UV-absorbance detection was achieved at 254 nm. The capillary temperature was maintained at 25 °C and the instrument was utilized at all times per manufacturer recommendations. A schematic illustration of the commercial CE instrumentation is shown in Figure 3.1.

3.4.2 Microchip Electrophoresis Instrumentation

Microchip separations were performed on the fused-silica microchip device with etched "bubble cell" and UV-absorbance, spectral detection system described in Chapter 2. A Bertan/Spellman high-voltage power supply (0 – 10 kV) coupled to an array of high-voltage relays, built in-house, was used to perform sample injection and separation.

Briefly, gated flow is established by applying potentials at each reservoir such that an interfacial region (cross) is developed and maintained at the intersection of the microchip arms and the flux of sample material is confined exclusively from sample reservoir (SR) to sample waste (SW). Sample is injected by momentarily altering the gate potentials, such that materials is temporarily allowed to enter the buffer reservoir (BR) & buffer waste (BW) arms, thus filling the cross. Gate potentials are then re-established and sample

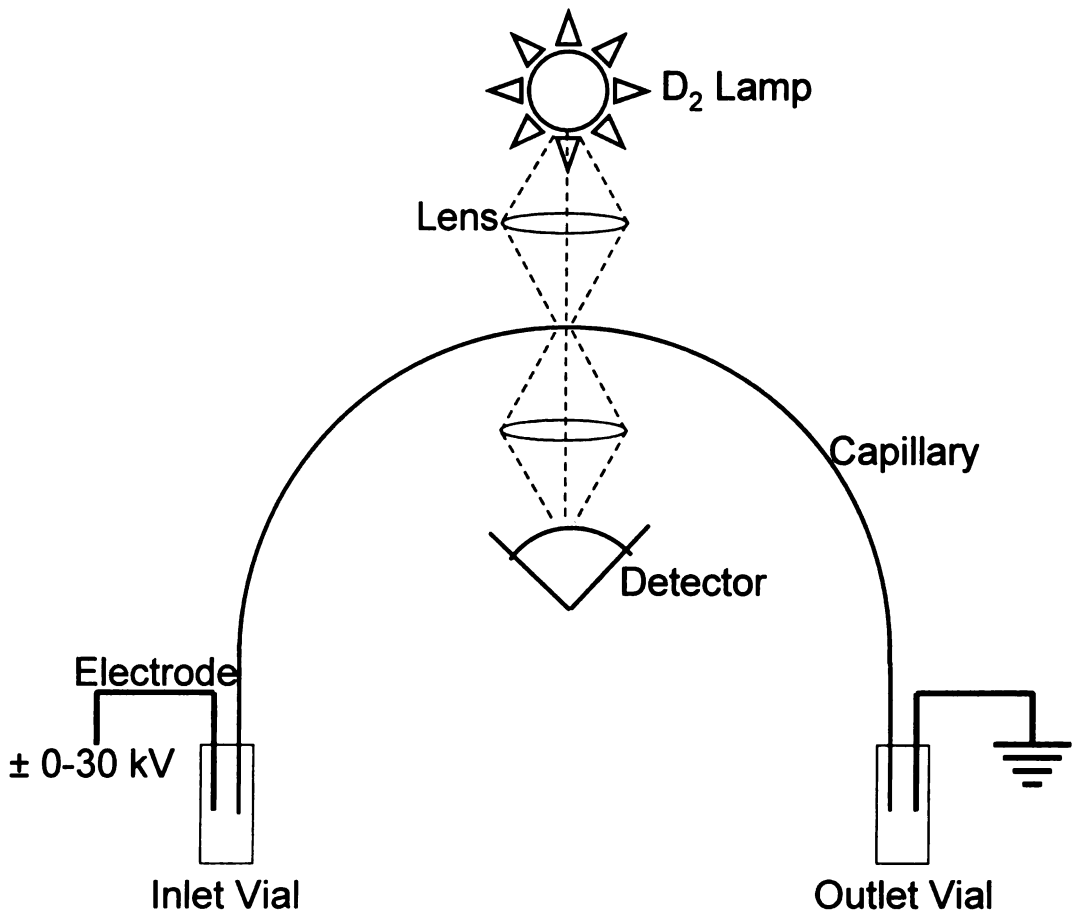

Figure 3.1: Schematic illustration of Beckman P/ACE Capillary Electrophoresis system used for capillary MEKC separations.

material in the cross undergoes separation as it travels down the BW arm. The gate and injection potentials used in this study are identified with their respective figures.

Computer control of the high-voltage power supply and relays as well as data collection and storage was achieved via LabView programming written in-house. Briefly, computer control of the high-voltage power supplies enabled simultaneous and independent control of each electrode used to dictate flow in the microchip device. Data collection and storage was achieved on a second computer via the program described in Chapter 2.

3.5 *Data Treatment and Analysis.*

Raw data from the microchip electrophoresis device were imported into a commercially available spreadsheet application (Excel, Microsoft Corp., Redmond, WA) and subjected to a 15-point moving average to attenuate random noise prior to generating electropherograms.

CHAPTER 4

RESULTS AND DISCUSSION

4.1 *UV-Absorbance Spectra.*

Molecular structures and UV absorbance spectra (210 – 400 nm) of the four alkaloids of interest are shown in Figure 4.1. It is clear that a primary absorption band between 210 – 300 nm exists for each analyte; however, only colchicine exhibits an appreciable secondary absorption band above 300 nm. Unfortunately, microchips fabricated from soda lime glass do not transmit UV light below ~ 320 nm. Therefore, it was necessary to fabricate microchips from UV-transparent fused-silica. Additionally, it is clear that each of these molecules is neutral above pH 7 and will co-migrate with electroosmotic flow under typical CE conditions. For this reason, micellar electrokinetic chromatography (MEKC) was selected to achieve separation on the microchip.

4.2 *Method Development.*

Background electrolyte (borate-cholate, TRIS-cholate, borate-SDS, and TRIS-SDS) and sample matrix (NaOAc, $Na_2B_4O_7$, and NaCl) compositions for capillary-MEKC separations of a series of 10 alkaloids with improved sensitivity via micelle stacking have recently been investigated by Giordano et al. [45]. These studies illustrated that: (1) micelle stacking is a phenomenon that is ubiquitous to conditions traditionally attributed to apparently disparate pre-concentration techniques; (2) the dynamic nature of micelle stacking is dictated

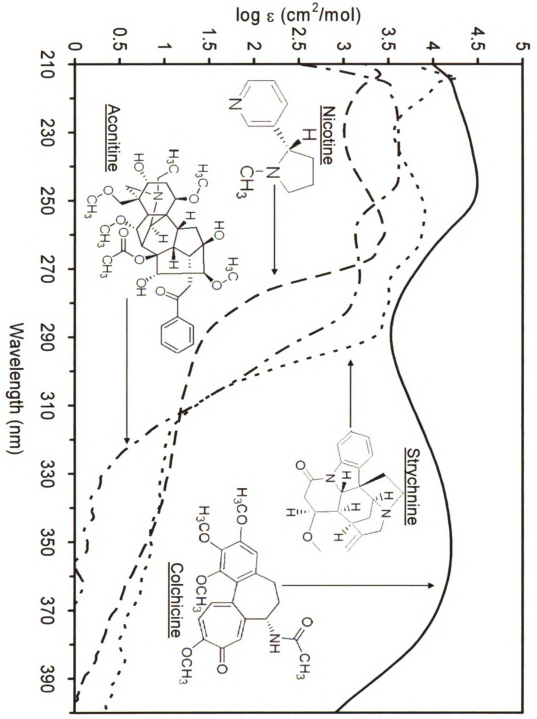

Figure 4.1: Molecular structures and UV-absorbance spectra (210 – 400 nm) of aconitine, colchicine, nicotine, and strychnine (0.7 – 500 μM) obtained with Hitachi double-beam U-3000 spectrophotometer.

by the nature and concentration of the sample matrix and background electrolyte; (3) cholate-containing background electrolytes facilitate greater micelle stacking than do SDS-containing background electrolytes and; (4) the greatest extent of micelle stacking is achieved with the NaOAc sample matrix in TRIS-cholate whereas, the greatest dynamic range is observed in borate-cholate. Table 4.1 lists the sample matrix and background electrolyte conditions under which optimum micelle stacking was achieved [45].

Figure 4.2 illustrates CE separations of 10 alkaloids performed with the BGE and sample matrix conditions identified in Table 4.1. Each of these separations was performed with relatively long (45 mm) injection lengths and short (15 cm) separation distances – the same distances under which maximum micelle stacking was achieved. Panels A through D correspond to separations performed in borate-cholate, TRIS-cholate, borate-SDS, and TRIS-SDS, respectively. The bottom trace in each panel shows the electropherogram obtained via traditional MEKC, in which there is no micelle stacking. The remaining traces in each panel correspond to separations achieved with $Na_2B_4O_7$, NaOAc, and NaCl sample matrices (bottom to top, respectively). It is apparent that, although no separation is achieved via traditional MEKC, each of the conditions which promote micelle stacking yields some (albeit poor) extent of separation and analyte enrichment.

Figure 4.3 illustrates separations of the same 10 alkaloids performed under conditions which afford optimum analyte enrichment and resolution. These sample matrix conditions are also listed in Table 4.1. Panels A through D

Table 4.1: Background electrolyte, sample matrix, and calculated percent increase in micelle concentration for maximum micelle stacking as well as sample matrix compositions for optimal enrichment and resolution.

BGE	Sample Matrix (Optimal Micelle Stacking)	% Increase in Micelle Concentration	Sample Matrix (Optimal Analyte Separation)
borate-cholate	40 mM $Na_2B_4O_7$	582	25 mM $Na_2B_4O_7$
	100 mM NaOAc	1038	100 mM NaOAc
	300 mM NaCl	618	90 mM NaCl
TRIS-cholate	20 mM $Na_2B_4O_7$	320	20 mM $Na_2B_4O_7$
	80 mM NaOAc	3360	80 mM NaOAc
	80 mM NaCl	919	70 mM NaCl
borate-SDS	11 mM $Na_2B_4O_7$	204	10 mM $Na_2B_4O_7$
	80 mM NaOAc	317	80 mM NaOAc
	10 mM NaCl	34	40 mM NaCl
TRIS-SDS	10 mM $Na_2B_4O_7$	77	10 mM $Na_2B_4O_7$
	10 mM NaOAc	245	10 mM NaOAc
	15 mM NaCl	39	15 mM NaCl

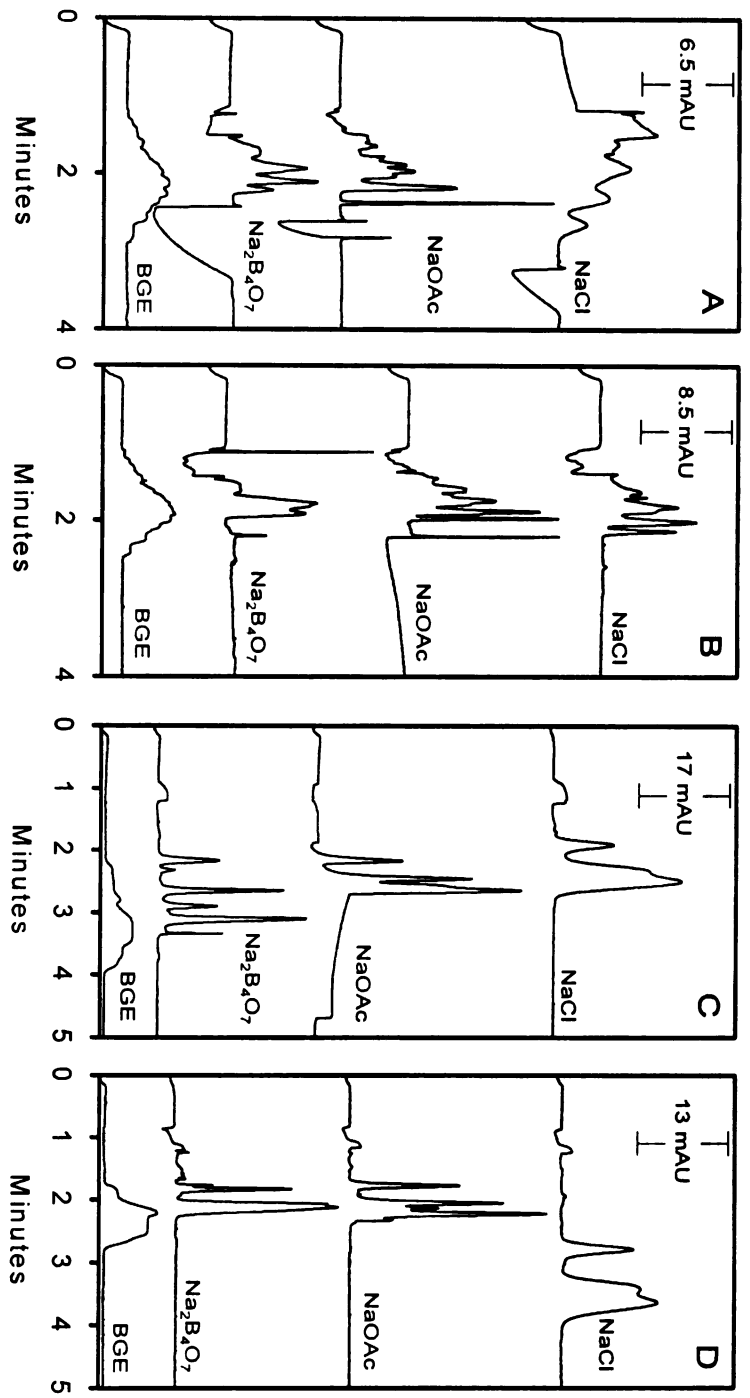

Figure 4.2: Effect of optimal micelle stacking condition on the separation of 10 alkaloids. Experimental conditions: Total length = 31 cm (15 cm effective length), l_{inj} = 45 mm, V = 15 kV, UV-absorbance at 254 nm. BGE = borate-cholate (A), TRIS-cholate (B), borate-SDS (C), and TRIS-SDS (D). Concentrations of $Na_2B_4O_7$, NaOAc, and NaCl sample matrices as listed in Table 4.1.

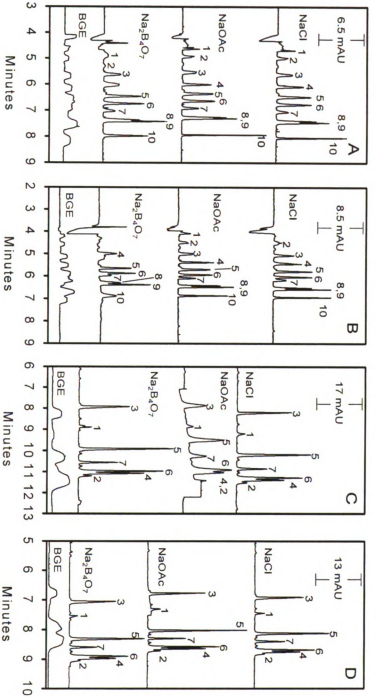

Figure 4.3: Effect of optimized sample enrichment on the separation of 10 alkaloids: 43 mM nicotine (1) and aconitine (2), 13 mM colchicoside (3), 17 mM strychnine (4), 13 mM thiocolchicoside (5), 17 mM colchicine (6) and 13 mM benzion methyl ether (7), yohimbine (8), thiocolchicine (9), and emetine (10). Experimental conditions: Total length = 31 cm (45 cm effective length), l_{inj} = 20 mm, V = 25 kV, UV-absorbance at 254 nm. BGE = borate-cholate (A), TRIS-cholate (B), borate-SDS (C), and TRIS-SDS (D). Concentrations of $Na_2B_4O_7$, NaOAc, and NaCl sample matrices as listed in Table 4.1.

correspond to separations performed in borate-cholate, TRIS-cholate, borate-SDS, and TRIS-SDS, respectively. The bottom trace in each panel shows electropherograms obtained via traditional MEKC. The remaining traces in each panel correspond to separations achieved with $Na_2B_4O_7$, NaOAc, and NaCl sample matrices (bottom to top, respectively).

It is apparent that most of the BGE and sample matrix compositions are identical; whereas, injection lengths and separation distances are substantively different. The injection and separation lengths used in Figure 4.2 are 45 mm and 15 cm, respectively, which provide for electronic conditions (e.g. relative conductivity and length) appropriate to optimally stack micelles. Unfortunately, these conditions do not provide adequate distance to facilitate separation. Conversely, the injection and separation lengths used to create Figure 4.3 are 20 mm and 45 cm, respectively, which provide sufficient distance to achieve separation and facilitate analyte interaction with stacked micelles, but do not provide the appropriate electronic conditions for optimal micelle stacking. It is also evident that better analyte enrichment is achieved in the SDS-containing background electrolytes; whereas, better resolution is achieved in the cholate-containing background electrolytes. These trends comport reasonably well with the expected relative partition coefficients for these analytes in cholate and SDS.

The steroid-like structure of cholate surfactant monomers (Figure 4.4A) supports retention in aqueous environments that is dominated by hydrogen-bonding and supported by dispersion interactions. Here, cholate micelles are characterized by a dynamic aggregation of ~ 20 monomers into loose, ball-like

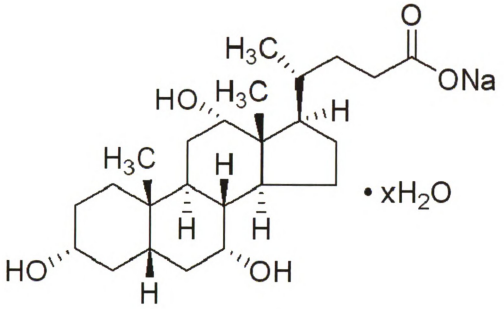

Figure 4.4A: Molecular structure of sodium cholate – hydrate monomer.

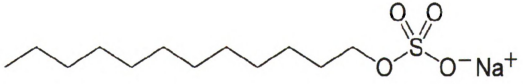

Figure 4.4B: Molecular structure of sodium dodecyl sulfate monomer.

structures [53], resulting in a broad range of partition coefficients for these analytes. However, cholate micelles do not solvate alkaloids as efficiently as SDS; resulting in a fairly broad range of partition coefficients for these analytes, as evidenced in Figure 4.3.

Conversely, the amphiphilic structure of SDS surfactant monomers (Figure 4.4B) supports retention in aqueous environments that is dominated by dispersion interactions. Here, SDS micelles are characterized by dynamic aggregation of ~ 60 monomers into tight, ball-like, lipid structures; polar head-groups oriented outward and non-polar tail-groups oriented inwards [54]. This orientation serves to effectively solvate analyte molecules within the hydrophobic micellar core and results in large partition coefficients for poorly water-soluble alkaloids, but does not necessarily afford a wide separation window.

4.2.1 Evidence of Micelle Stacking in Microchip-MEKC.

The BGE and sample matrix conditions that were observed to produce optimized analyte separation and enrichment via micelle stacking in capillary-MEKC were transitioned to the microchip platform by determining appropriate voltages to achieve reproducible gated injections. However, due to fundamental differences between the normal modes of sample injection for capillaries (hydrodynamic) and microchips (gated, electrokinetic), it was important to first verify that the same conditions which produce micelle stacking in a capillary also produce micelle stacking in a microchip.

In order to provide evidence of micelle stacking in microchip-MEKC, the borate-cholate BGE was prepared with 50 μM Sudan III as a micelle marker [55]. Sample matrices of 100 mM NaOAc, 25 mM $Na_2B_4O_7$, and the BGE without Sudan III were prepared and injected onto the microchip via gated injection. This is the same procedure performed by Giordano and co-workers to demonstrate the presence of stacked micelles in capillary MEKC [45].

Figure 4.5 shows the effect of sample matrix on micelle stacking in microchip-MEKC. It is apparent that when the BGE without Sudan III is injected as a sample matrix, only a vacancy peak corresponding to the absence of dye is observed. However, it is also demonstrated that when either the NaOAc or $Na_2B_4O_7$ sample matrix is injected, there is a narrow region of increased micelle concentration (re: micelle stacking), that is immediately followed by a vacancy peak.

The intensity of the stacked micelle band achieved with the $Na_2B_4O_7$ sample matrix is approximately twice that achieved with the NaOAc sample matrix, whereas the width of the vacancy peak is roughly the same, regardless the extent of micelle stacking. This discrepancy between the heights of the stacked micelle bands at the NaOAc and $Na_2B_4O_7$ interfaces results from the confluence of multiple contributions. Most dominant of these are the different relative conductivities & lengths of the NaOAc and $Na_2B_4O_7$ sample matrices when compared to the BGE as well as different rates at which the stacked micelle regimes evolve between these sample matrices [45]. More importantly, these results verify the presence of micelle stacking in microchip-MEKC.

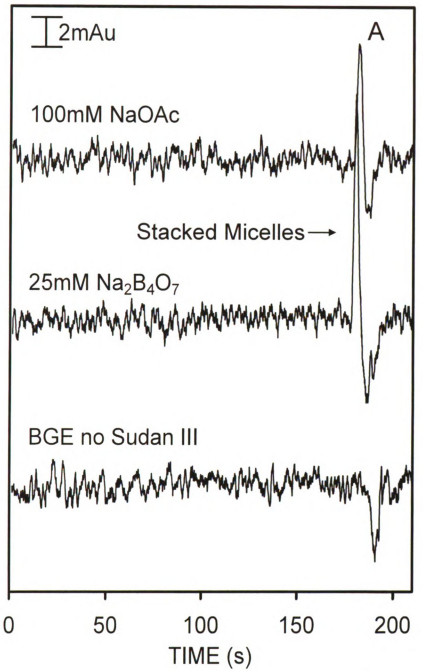

Figure 4.5: Effect of sample matrix on micelle stacking in MEKC. Experimental conditions: BGE = borate-cholate + 50μM Sudan III. Sample matrix: 100mM NaOAc (top); 25mM $Na_2B_4O_7$ (middle); borate-cholate (bottom). Gate potentials: SR/SW/BR/BW = 1.8/1.0/2.0/0kV. Injection: 5 sec BR float. UV-absorbance detection at 252 nm.

4.2.2 Effects of Micelle Stacking on Analyte Enrichment in Microchip-MEKC.

In order to identify the potential utility of on-line preconcentration in microchip-MEKC for analyte enrichment, 50 μM Rhodamine B was prepared in 100 mM NaOAc, 25 mM $Na_2B_4O_7$, and BGE. Figure 4.6 shows the effect of sample matrix on analyte enrichment in microchip-MEKC. It is apparent that a peak for Rhodamine B is observed for each of the sample matrices. However, it is also shown that the sample matrix which yielded the greatest extent of micelle stacking (25 mM $Na_2B_4O_7$, Figure 4.5) provides no improvement in sensitivity over the BGE. In contrast, a roughly two-fold increase in sensitivity is observed for the 100 mM NaOAc sample matrix, despite exhibiting a less substantial extent of micelle stacking. This discrepancy between the extent of micelle stacking and the extent of analyte enrichment has been shown to arise from a time-dependence of the micelle stacking phenomenon. Generally, the NaOAc sample matrix facilitates more rapid micelle stacking than the $Na_2B_4O_7$ sample matrix [45]. This trend, coupled with the transient interaction of analytes with the stacked micelle region while traveling from the sample matrix to the BGE, results in more efficient enrichment for analytes prepared in the NaOAc sample matrix than in the $Na_2B_4O_7$ sample matrix. The above trends for the extent of micelle stacking and analyte enrichment have also shown to be consistent with the TRIS-cholate BGE system by CE (data not shown).

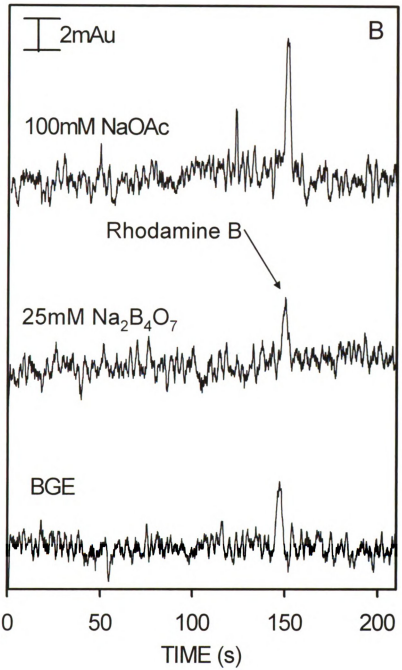

Figure 4.6: Effect of sample matrix on analyte enrichment in microchip-MEKC. Experimental conditions: Sample matrices same as Figure 4.5 + 50μM Rhodamine B. All other conditions same as Figure 4.5.

4.3 *Microchip-MEKC Separations of Alkaloids.*

Unfortunately, most of the conditions for optimal analyte separation listed in Table 4.1 did not translate successfully to the microchip platform. For example, NaCl sample matrices have no substantive buffering capacity and are therefore incapable of reproducible, gated injections. Additionally, SDS-containing BGE exhibit significantly larger conductivities than any of the sample matrices identified in Table 4.1 as to altogether preclude gated injections. For these instances, sample matrix compositions were modified to facilitate gated injections, but at the inevitable loss of resolution. This is perhaps best illustrated in Figure 4.7A and Figure 4.7B.

Here, the sample matrix has been increased from 10 mM $Na_2B_4O_7$ to 20 mM $Na_2B_4O_7$ in order to support gated injections. Figure 4.7A demonstrates that substantial analyte enrichment is achieved for injections of 50 uM Rhodamine B in borate-SDS from 2 – 60 seconds. However, Figure 4.7B illustrates that the overall separation of the alkaloid mixture is quite poor in 20 mM $Na_2B_4O_7$.

On the other hand, separations in both the TRIS-cholate and the borate-cholate BGE systems with NaOAc sample matrices (80 and 100 mM, respectively) were observed to translate best from the capillary to the microchip. Of these, greater resolution and sensitivity was achieved in the TRIS-cholate BGE with 80 mM NaOAc sample matrix.

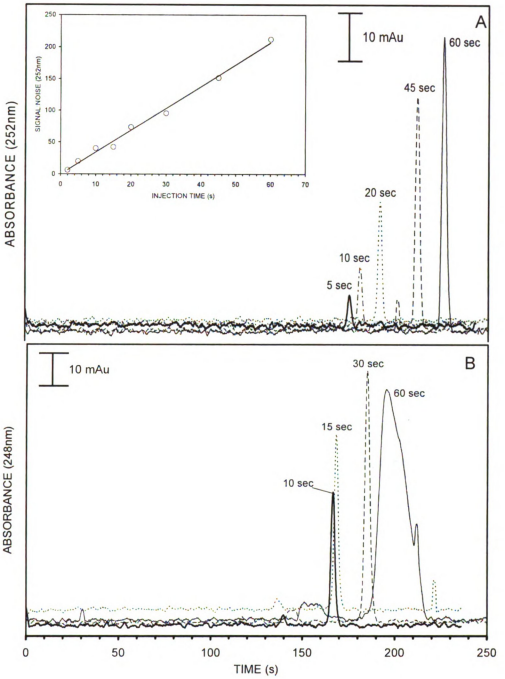

Figure 4.7: Example of background electrolyte and sample matrix conditions that translated poorly to the microchip platform. Experimental conditions: BGE = borate-SDS; sample matrix = 50 μM RhB (A), 100 μM nicotine, aconitine, strychnine, and cholchicine (B) in 20 mM $Na_2B_4O_7$. Gate potentials: SR/SW/BR/BW = 1.8/1.0/2.0/0kV. Injection Time = 2 – 60 seconds. UV-absorbance at 252 nm (A) and 248 nm (B).

4.3.1 Effects of Micelle Stacking.

Figure 4.8 shows microchip-MEKC separations of aconitine, colchicine, nicotine, and strychnine in TRIS-cholate BGE with TRIS-cholate (bottom trace) and NaOAc (top trace) sample matrices. It is evident that migration times are not influenced by the enrichment process, and that greater sensitivity is achieved in the NaOAc sample matrix than with conventional MEKC. It is also apparent that although greater signal is achieved for each analyte under micelle stacking conditions, there is a general trend of increasing enrichment with increasing retention. Thus, later eluting analytes experience greater enrichment than earlier eluting analytes, consistent with trends previously observed by Terabe and Palmer [34,37]. This is because later eluting analytes have a higher affinity for the micelle and, consequently, spend more time interacting with the growing stacked micelle band than do earlier eluting analytes.

Figure 4.9 shows the effect of concentration on microchip-MEKC separations with micelle stacking. As expected, a monotonic decrease in signal with decreasing concentration is observed. It is also apparent that migration time varies negligibly (< 5%) with concentration, thereby, illustrating the run-to-run reproducibility of these separations. Additionally, comparison of the top trace with that in Figure 4.8 illustrates < 10% day-to-day variation in migration time and < 5% variation in detector response.

It is important to note that Figures 4.8 and 4.9 illustrate electropherograms collected at 248 nm. Inspection of Figure 4.1 shows that, although this wavelength is useful for detection of each analyte, no single wavelength between

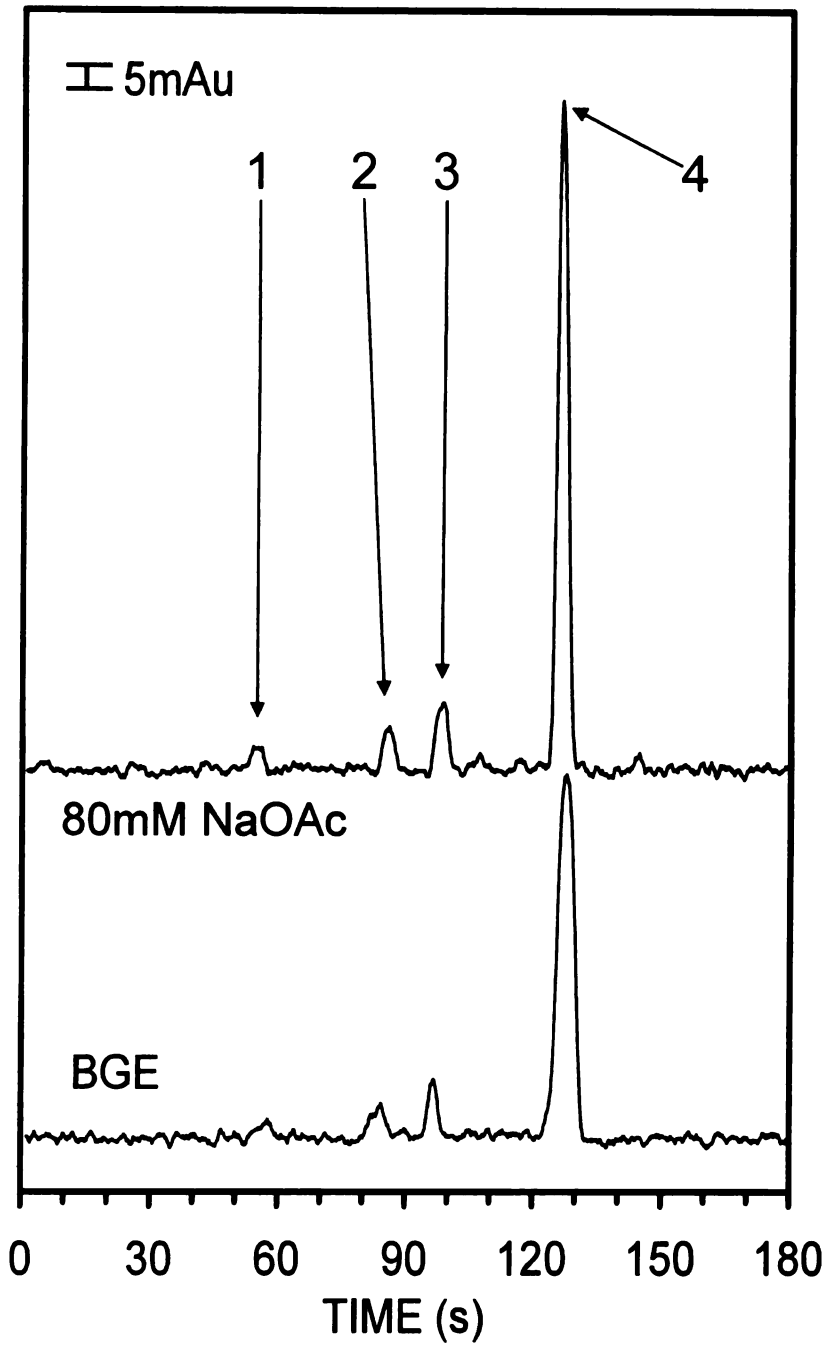

Figure 4.8: Effect of micelle stacking on microchip-MEKC separations of aconitine, cochicine, nicotine, and strychnine. Experimental conditions: BGE = TRIS-cholate; sample matrix: 500μM aconitine, colchicine, nicotine, and strychnine in 80mM NaOAc (top); BGE (bottom). Gate potentials: SR/SW/BR/BW = 2.7/1.5/3.0/0kV. Injection: 5 sec BR float. Typical operating current (BR – BW) ~50μA. UV-absorbance detection at 248 nm.

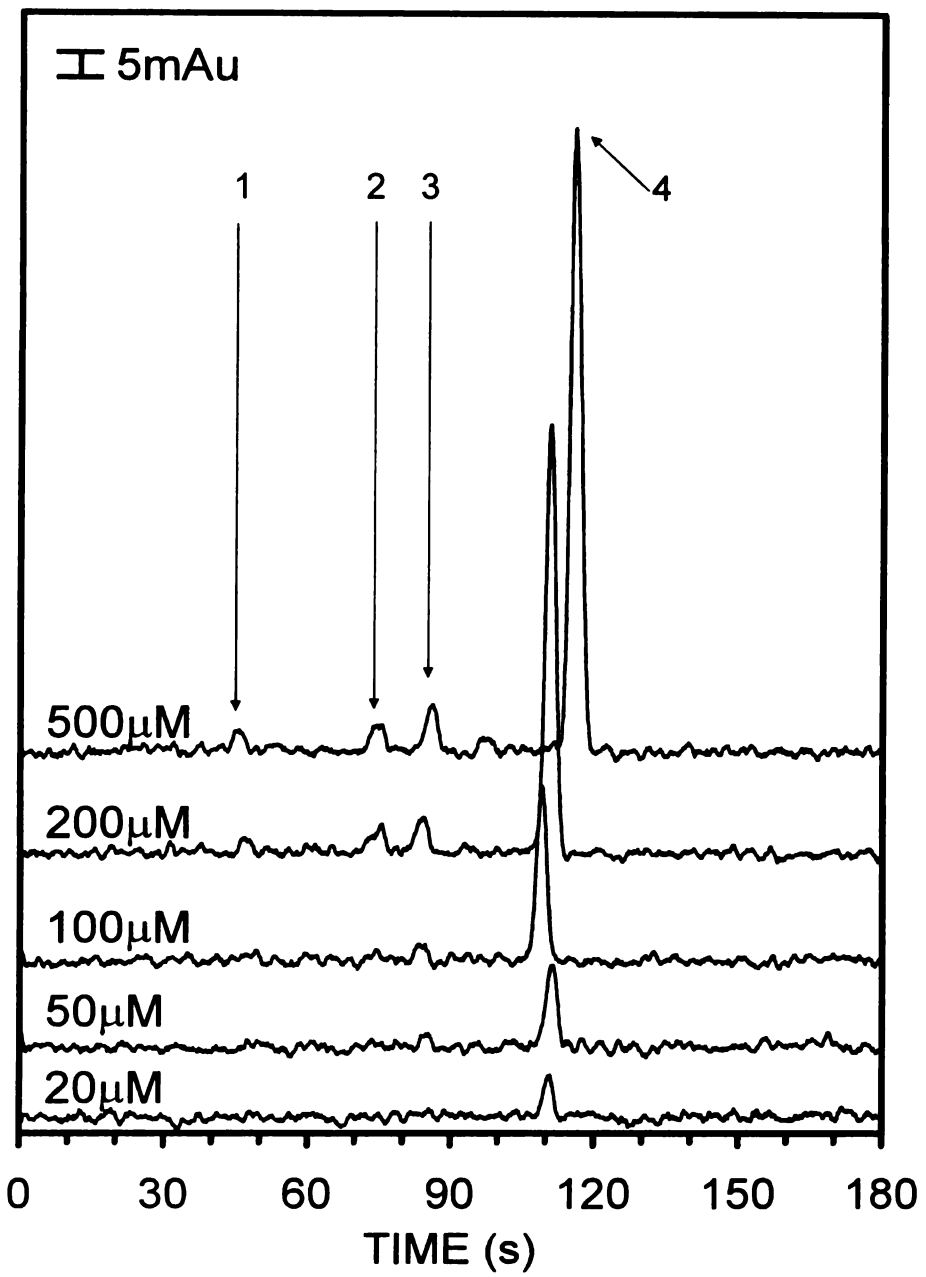

Figure 4.9: Effect of concentration on microchip-MEKC separations with micelle stacking. Experimental conditions: Experimental conditions: sample matrix = 20 – 500μM aconitine, colchicine, nicotine, and strychnine in 80mM NaOAc. All other conditions same as Figure 4.8.

210 and 400 nm is best for detecting all of the analytes. Thus, multi-wavelength detection is essential to achieve optimal sensitivity.

4.3.2 Effects of Detection Wavelength.

This statement is better illustrated in Figure 4.10 via a spectro-electropherogram of the microchip-MEKC separation of aconitine, colchicine, nicotine, and strychnine. Each trace represents the UV-absorbance signal measured simultaneously between 210 – 400 nm at ~4.5 nm intervals; the bold trace at 248 nm represents the top trace in Figure 4.8. It is apparent that although baseline resolution at 248 nm is achieved in less than 2 minutes, this wavelength does not provide the best sensitivity for any analyte. For example, nicotine was best detected at 261 nm, aconitine at 229 nm, strychnine at 252 nm, and colchicine at 243 nm (Table 4.2). It is also shown that the spectral UV-absorbance response of each analyte follows the same trends as those observed in Figure 4.1.

It is important to afford perspective when discussing the separation and detection of toxic substances. This is achievable by considering the ability to detect concentrations equivalent to a lethal dose. The Hodge and Sterner scale can be used to comparatively rate toxicity and LD_{50} values. LD_{50} values of 1 – 50 mg/kg are class 2 (highly toxic); whereas, LD_{50} values > 15,000 mg/kg are class 6 (relatively harmless). For example, aspirin has a rat LD_{50} ~ 200 mg/kg and is class 3 (moderately toxic) and cyanide has rat LD_{50} ~ 8 mg/kg and is class 2 (highly toxic). It is evident that whereas their structures vary considerably in

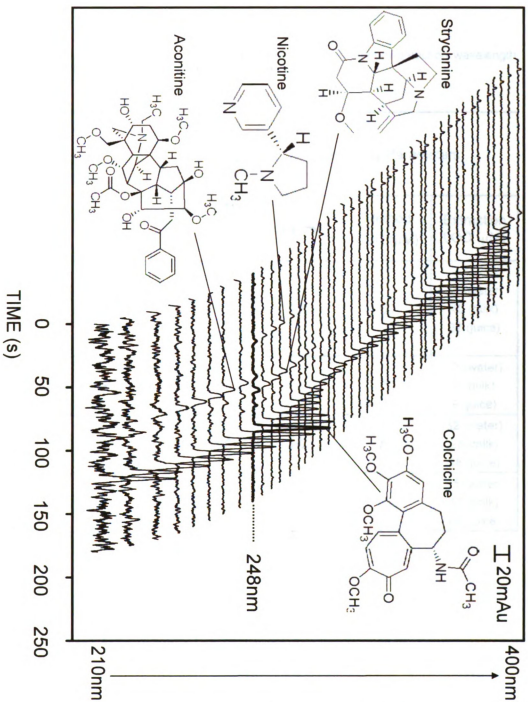

Figure 4.10: Effect of detection wavelength on sensitivity for the microchip-MEKC separation of aconitine, colchicine, nicotine, and strychnine. Experimental conditions: sample matrix = 500μM each aconitine, colchicine, nicotine, and strychnine in 80mM NaOAc. UV-absorbance detection at 210 – 400 nm. All other conditions same as Figure 4.9.

Table 4.2: Toxicity, lethal dosage, and sensitivity parameters (optimum detection wavelength, separation detection limit, and extraction detection limit).

	LD_{50} (rat) mg / kg	Lethal Dose (μM / 12 oz.) 50kg / 100kg	Sensitivity Parameters		
			λ (nm)	Method LOD (μM)	Extraction LOD (μM)
Aconitine	0.08	20 / 40	229	50	34 (water) 40 (milk) 32 (juice)
Colchicine	1.6	570 / 1140	243	20	12 (water) 9 (milk) 9 (juice)
Strychnine	2.35	990 / 1980	252	50	32 (water) 28 (milk) 38 (juice)
Nicotine	50	43529 / 87058	261	100	75 (water) 81 (milk) 86 (juice)

complexity, each of the proposed solutes is aromatic, absorbs UV light, and is highly toxic.

Table 4.2 also lists the LD_{50} values and the corresponding lethal dosage in a 12 oz liquid serving as well as the lowest concentration detected from linear regression ($R^2 > 0.99$) at the most sensitive wavelength for each alkaloid.

It is demonstrated that, as a consequence of the employed combination of instrument and method development, colchicine, strychnine, and nicotine are detected on a microchip device at concentrations that are 25 – 400 times more sensitive than a lethal dose for a 50 kg (~100 lb) individual. However, it is also apparent that, as a result of the extreme toxicity of aconitine, even detection as low as 50 μM is still greater than twice the lethal dose for a 50 kg individual.

4.4 *Microchip-MEKC Analysis of Alkaloids in Beverages.*

In the preceding section it was shown that, although good native sensitivity is demonstrated for each of these analytes via UV-absorbance detection, improvements in sensitivity are still necessary. These improvements can likely be gained by employing sample preparation methods such as SPE when confronted with real samples.

In order to demonstrate this, 10 mL samples of water, apple juice, and fat-free milk were spiked with 30 μM of each alkaloid and subjected to the solid phase extraction procedure described in Chapter 3. Additionally, two blank extractions were performed with uncontaminated water. The eluent of one blank extract was then spiked with 60 μL of each 5 mM alkaloid stock solution and then

blown to dryness to serve as a known standard for comparison. Evaporated extracts were reconstituted in 0.6 mL of 80 mM NaOAc to yield 500 μM of each alkaloid, assuming 100% recovery. A blank extract was injected prior to each alkaloid-containing sample in order to eliminate cross-contamination. The extraction procedure was reproducible to between 3 – 4% RSD (n > 3).

Figure 4.11A shows electropherograms of the recovery from the water, juice, and milk extractions as well as the extract blank and standard. Although the electropherogram of the blank extract is absent of interfering species, migration times in the standard have increased marginally (~40 seconds) relative to separations of the same alkaloids in Figure 4.8. This may be a result of the presence of undetected ionic, stationary-phase species removed from the silica support of the SPE cartridge as a consequence of acidifying the sample matrix with 10% v/v of 1 M HNO_3. Peaks for strychnine and colchicine are clearly visible at 248 nm in separations of the water, milk, and juice extracts; however, recovery of nicotine and aconitine are less obvious at this wavelength. Figures 4.11B and 4.11C show the UV absorbance spectra and peaks for nicotine and aconitine (respectively) at the wavelengths indicated in Table 4.2. These data highlight the benefit of employing spectral detection methods to identify otherwise undetected analytes.

Table 4.2 also lists the extract detection limits of each alkaloid at the wavelengths identified from water, milk, and juice extracts versus the 500 μM standard. Extraction LOD values were extrapolated by augmenting the standard LOD for the method by the calculated percent recovery from extraction by:

Figure 4.11: Microchip-MEKC separations (A) of SPE extracts of blank and 500 μM standard as well as tap water, skim milk, and apple juice spiked to 30 μM each alkaloid (nicotine, aconitine, strychnine, and colchicine) and reconstituted to 500 μM, assuming 100% recovery in 80 mM NaOAc. All other conditions same as Figure 4.9. UV-absorbance spectra of nicotine (B) and aconitine (C) shown for Milk extract separation. Insets correspond to peaks for nicotine (261 nm) and aconitine (229 nm).

Extraction LOD = Standard LOD x (100% – Percent Recovery) / 100 (6)

It is important to note that this calculation assumes that the percent recovery from extraction is linear with initial concentration.

These data show that, in general, colchicine experiences the best recovery (40 – 56%) from each beverage; whereas, nicotine experiences with worst recovery (14 – 25%). This discrepancy in extraction efficiency between analytes is due to their differences in affinity for the strong-cation exchange / partition stationary phase material relative to that of the sample, wash, and elution mobile phases. These recoveries are not as substantial as those reported recently by Jablonski et al. (nicotine ~ 72%, strychnine ~ 78%, and aconitine ~ 83%) [56]; however, they do represent a substantial improvement in simplicity as well as overall analysis time (< 10 minutes vs ≥ 1 hour). This advantage notwithstanding, investigations to improve extraction efficiencies to more closely resemble those by Jablonski et al. are on going.

CHAPTER 5

CONCLUSIONS & FUTURE DIRECTIONS

5.1 *CONCLUSIONS*

The development of a CE microchip device with UV-absorbance spectral detection is described and its successful application to the separation, detection, and identification of toxic alkaloids at or below lethal dosages is demonstrated. This was achieved by a combination of instrumental and experimental design that included the focusing and collection of UV light through an etched "bubble cell" in a fused-silica microchip, as well as application of on-line analyte enrichment via micelle stacking. A miniature CCD spectrometer was used to detect UV light and software was written in-house to simultaneously monitor and record separations from 210 – 400 nm. This detection scheme enabled both qualitative and quantitative separations to be achieved by resolving solutes spatially, as well as spectrally. It is also demonstrated that, in addition to improved resolution and analyte identification, spectral detection affords enhanced sensitivity over single-wavelength detection. Moreover, sensitive and selective UV-absorbance detection is easily achieved on a CE microchip device. Thus, microchip separations can effectively be applied to a more broad and interesting range of molecules; not necessarily being limited to those that fluoresce or are electrochemically active.

This versatility was used to demonstrate that low concentration detection limits are achievable on the microchip platform for colchicine and strychnine,

≥ 25μM (10ppm and 8ppm, respectively); aconitine, ≥ 50mM (38ppm); and nicotine, ≥ 100μM (16ppm). With the exception of aconitine, these concentrations are 25 – 400 times more sensitive than what is required to detect a lethal dose. Finally, the developed microchip device and experimental methods were combined with a simple, solid-phase extraction method to successfully detect all four alkaloids in water, fat-free milk, and apple juice samples spiked with sub-lethal dose concentrations. Although the demonstrated gains in sensitivity extend the useful range of microchip separations, further investigation of on-line pre-concentration techniques is warranted.

The net contribution of this work to forensic science is two-fold. First, and foremost, it has been demonstrated that a microchip device can be designed and successfully applied to achieve rapid separation and true UV-absorbance detection. Moreover, because detection is achieved by simultaneous collection of UV-absorbance spectra, it is demonstrated that analyte spectral identification is also possible with this device. Cumulatively, these milestones expand the realm of microchip separations to include a broader and more interesting range of molecules; no longer limited to those that fluoresce or are electrochemically active. This means that the same microchip device now has the potential for use to test for a range of different substances (i.e. nitroaromatics, opiates, barbiturates, etc.) without physically altering the device or chemically modifying the samples. Second, due to the compact nature of the microchip and operating components, there is real and viable potential to translate this device onto a platform that is truly portable. Such a transition will enable rapid, on-site testing

and evaluation of suspect substances, thereby facilitating protection of public health.

5.2 *FUTURE DIRECTIONS*

However, in order for the development of such a device to achieve fruition, further work is needed in miniaturizing the supporting instrumental architecture to the extent that all of the components fit and operate within a field-portable container. This includes multi-channel power supplies and light sources as well as detection optics and microchip stage. Additional development of separation and extraction procedures is also important to expand the range of target analytes that can be analyzed.

All told, the continued development towards miniaturized separation platfoms coupled with the utility of UV-absorbance spectral detection and a standardized approach for sampling and separation will provide a powerful tool to support public safety measures by facilitating rapid, in situ screening of foods and beverages for toxin contamination.

REFERENCES

1. G. Hamscher; B. Priess; H. Nau; E. Panariti *Anal. Chem.* **2005**, *77*, 2421-2425

2. S. Sannohe; Y. Makino; T. Kita; N. Kuroda; T. Shinozuka *J. Forensic Sci.* **2002**, *47*, 1391-1396

3. V. C. Danel; J. F. Wiart; G. A. Hardy; F. H. Vincent; N. M. Houdret *J. Toxicol. Clin. Toxicol.* **2001**, *39*, 409-411

4. H. Ohta; Y. Seto; N. Tsunoda *J. Chromatogr. B* **1997**, *691*, 351-356

5. F. A. Carey *Organic Chemistry*, 6th ed., New York: McGraw Hill, **2006**

6. www.wikipedia.com, **2007**

7. D. M. Hostege; J. N. Seiber; F. D. Galey *J. Agric. Food Chem.* **1995**, *43*, 691-699

8. K. Wada; H. Bando; N. Kawahara; T. Mori; M. Murayama *Biol. Mass Spec.* **1994**, *23*, 97-102

9. Y. Gaillard; G. Pepin *J. Chromatogr. B.* **1999**, *733*, 181-229

10. V. K. Moore; M. E. Zabik; J. M. Zabik *Food Chem.* **2000**, *71*, 443-447

11. H. H. Maurer *Clin. Biochem.* **2005**, *38*, 310-318

12. Ong, E. S.; Apandi, S. N. B. *Electrophoresis* **2001**, *22*, 2723-2729

13. H. T. Feng; S. F. Y. Li *J. Chromatogr. A* **2002**, *973*, 243-247

14. J. Y. Zhang; S. F. Wang; X. G. Chen; Z. D. Hu; X. Ma *Anal. Bioanl. Chem.* **2003**, *376*, 210-213

15. A. Tiselius *Thesis: Nova Acta Regiae Societatis Scientiarum Uppsaliensis*, ser. IV, vol 7, Almqvist & Wiksell, Upsala, Sweden, **1930**

16. A. Tiselius *Trans. Faraday Soc.* **1937**, 33, 524

17. S. Hjerten *Chromatogr. Rev.* **1967**, *9*, 122

18. J. W. Jorgenson; K. D. Lukacs *Anal. Chem.* **1981**, *53*, 1298

19. Y.-S. Fung; H.-S. Tung *Electrophoresis*, **1999**, *20*, 1832

20. H. J. Issaq *Electrophoresis*, **2000**, *21*, 1921

21. X. M. Li; N. F. Hu; S. C. Lin *Anal. Letters* **1995**, *28*, 2203-2217

22. E. A. Kasim *Anal. Letters* **2002**, *35*, 1987-2004

23. R. Jindal; S. M. Cramer *J. Chromatogr. A* **2004**, *1004*, 277-285

24. Z. Liang; N. Chiem; G. Ocvirk; T. Tang; K. Fluri; D. J. Harrison *Anal. Chem.* **1996**, *68*, 1040-1046

25. H. Salimi-Moosavi; Y. Jiang; L. Lester; G. Mckinnon; D. J. Harrison *Electrophoresis* **2000**, *21*, 1291-1299

26. K. B. Morgensen; N. J. Peterson; J. Hubner; J. P. Kutter *Electrophoresis* **2001**, *22*, 3930-3938

27. G. E. Collins; Q. Lu *Anal. Chim. Acta* **2001**, *436*, 181-189

28. G. E. Collins; Q. Lu *Sensors and Actuators B* **2001**, *76*, 244-249

29. G. E. Collins; Q. Lu; N. Pereira; P. Wu *Talanta* **2007**, *72*, 301-304

30. Q. Lu; C. L. Copper; G. E. Collins *Anal. Chim. Acta* **2006**, *572*, 205-211

31. B. C. Giordano; A. Terray; G. E. Collins *Electrophoresis* **2006**, *27*, 4295-4302

32. Z. Liu; P. Sam; S. R. Sirimanne; P. C. McClure; J. Grainger; D. G. Patterson *J. Chromatogr. A* **1994**, *673*, 125-132

33. J. P. Quirino; S. Terabe *Science* **1998**, *282*, 465-467

34. J. P. Quirino; S. Terabe *Anal. Chem.* **1998**, *70*, 1893-1901

35. J. P. Quirino; S. Terabe *Anal. Chem.* **1998**, *70*, 149-157

36. J. Palmer; N. J. Munro; J. P. Landers *Anal. Chem.* **1999**, *71*, 1679-1687

37. J. P. Quiino; S. Terabe; P. Bocek *Anal. Chem.* **2000**, *72*, 1934-1940

38. J. Palmer; J. P. Landers *Anal. Chem.* **2000**, *72*, 1941-1943

39. Y. Sera; N. Matsubara; K. Otsuka; S. Terabe *Electrophoresis* **2001**, *22*, 3509-3513

40. J. Palmer; D. S. Burgi; N. J. Munro; J. P. Landers *Anal. Chem.* **2001**, *73*, 725-731

41. J. Palmer; D. S. Burgi; J. P. Landers *Anal. Chem.* **2002**, *74*, 632-638

42. Y. Liu; R. S. Foote; S. C. Jacobson; J. M. Ramsey *Lab Chip* **2005**, *5*, 457-465

43. B. Jung; R. Bharadwaj; J. G. Santiago *Anal. Chem.* **2006**, *78*, 2319-2327

44. B. C. Giordano; C. I. D. Newman; D. S. Burgi; G. E. Collins *Anal. Chem.* **2007**, *accepted for publication*

45. D. M. Osbourn; D. J. Weiss; C. E. Lunte *Electrophoresis* **2000**, *21*, 2768-2779

46. J. P. Quirino; J.-B. Kim; S. Terabe *J. Chromatogr. A* **2002**, *965*, 357-373

47. J.-B. Kim; S. Terabe *J. Pharm. Biomed. Anal.* **2003**, *30*, 1625-1643

48. M. Urbanek; L. Krivankova; P. Bocek *Electrophoresis* **2003**, *24*, 466-485

49. R.-L. Chien *Electrophoresis* **2003**, *24*, 486-497

50. R.-L. Chien *Electrophoresis* **2003**, *24*, 486-497

51. H. Armandula *Laser Interferometer Gravitational Wave Observatory*, California Institute of Technology: Pasadena, CA, **2005**

51. H. Sugioka; Y. Moroi *Biochim. Biophys. Acta – Lipids and Lipid Metab.* **1998**, *1394*, 99-110

52. P. Lianos; R. Zana *J. Phys. Chem.* **1980**, *84*, 3339-3341

53. M. R. N. Monton; K. Otsuka; S. Terabe *Journal of Chromatography A* **2003**, *985*, 435-445

54. J. E. Jablonski; J. E. Schlesser; P. Mariappagoudar *J. Agric. Food Chem.* **2006**, *54*, 7460-7465